Water Science & Technology



Water Science & Technology Vol 86 No 3, 596 doi: 10.2166/wst.2022.210

# Real-time monitoring of aqueous $Hg^{2+}$ reduction dynamics by magnetite/iron metal composite powders synthesized hydrothermally

Fabrice Brunet[a,*], Delphine Tisserand[a], Martine Lanson[a], Benjamin Malvoisin[a], Mathieu Bertrand[b] and Céline Bonnaud[b]

[a] ISTERRE, Univ. Grenoble Alpes, Univ. Savoie Mont Blanc, CNRS, IRD, Univ. Gustave Eiffel, Grenoble 38000, France
[b] HYMAG'IN, Grenoble 38000, France
*Corresponding author. E-mail: fabrice.brunet@univ-grenoble-alpes.fr

FB, 0000-0002-0929-8398

## ABSTRACT

An iron-based powder material composed of zerovalent iron (8 wt.%) and magnetite (92 wt.%), has been synthesized hydrothermally at 200 °C from zero-valent iron. Its effect on the reduction of aqueous $Hg^{2+}$ into gaseous $Hg^0$ has been investigated at ambient conditions for pH comprised between 4 and 8.5. The production of $Hg^0$ was monitored with an online mercury vapor analyzer at the picogram level for concentrations of iron-based composite of a few tenths of mg $L^{-1}$. Starting from a solution having an $Hg^{2+}$ concentration of 25 ng $L^{-1}$ at pH = 4, a succession of two $Hg^0$ production events was recorded. The first event is related to the $Hg^{2+}$ reduction by ZVI which fully dissolved within the first hours. Upon ZVI consumption, pH drifted towards the pH window where magnetite can efficiently reduce $Hg^{2+}$ at the hour timescale, resulting in a second $Hg^0$ production peak. The combined use of ZVI and magnetite to remove aqueous $Hg^{2+}$ by formation of $Hg^0$ (volatile) under mild acidic pH allows (1) to maximize the $Hg^{2+}$ reduction rate and (2) to take benefit of the longer lifetime of magnetite compared to ZVI.

**Key words:** CV-AAS, Hg reduction kinetics, Hg removal, steel-industry wastes, ZVI

## HIGHLIGHTS

- New experimental set-up for the in-situ monitoring of $Hg^0$ associated with aqueous $Hg^{2+}$ reduction by iron-based solid compounds.
- $Hg^0$ production bursts from a highly diluted $HgCl_2$ solution (25 ng $L^{-1}$) reacting with magnetite–zerovalent iron (ZVI) composite powder are monitored on a time-resolved basis.
- Magnetite and ZVI are efficient to reduce $Hg^{2+}$ in a different pH window.

## GRAPHICAL ABSTRACT

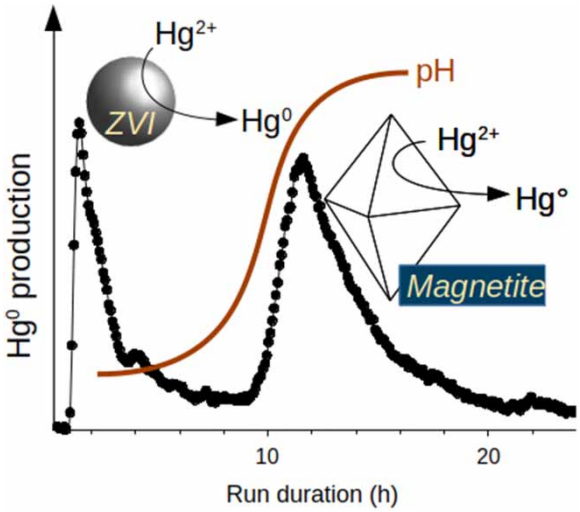

## INTRODUCTION

Simple iron-based compounds such as iron metal, iron oxides and hydroxides show a great potential for the removal of pollutants by various physico-chemical processes such as adsorptive removal or photocatalytic degradation (e.g. Mueller *et al.* 2012; Gusain *et al.* 2019; Gil-Díaz *et al.* 2021; Geneti *et al.* 2022). $Fe^{2+}$ and $Fe^0$ can also act as electron donors to convert the contaminant into a less soluble (Ponder *et al.* 2000; Crane *et al.* 2015) or a less toxic form (Zhang 2003; Liu & Wang 2019).

The steel industry produces hundreds of million tons of Fe-rich wastes yearly (Brunet 2019) that can be processed hydrothermally to obtain $Fe_3O_4$ nanoparticles (Crouzet *et al.* 2017). They can be valorized for the remediation of contaminated soils and groundwater. Here, the hydrothermal process proposed by Crouzet *et al.* (2017) to recycle ferrous wastes into nanomagnetite has been applied to a commercial powder of zerovalent iron (ZVI). The process was stopped before complete conversion of ZVI into magnetite, so that about 8 wt.% of ZVI remained unreacted. The recovered composite magnetite – ZVI product, called M/ZVI herein, was investigated for its capacity to reduce aqueous $Hg^{2+}$ over a range of pH comprised between 2 and 8.5. Indeed, Hg has been recognized as an element of global concern (UN Environment 2019). Mercury (Hg) bioaccumulates in the form of methylmercury which is highly neurotoxic to both human and aquatic systems (e.g. Clarkson & Magos 2006). Monomethylmercury, ($CH_3Hg^+$) is formed from $Hg^{2+}$ species under the activity of bacteria in anoxic media, the best known being iron- and sulfate-reducing bacteria as well as methanogens (Gilmour *et al.* 2013, 2018; Hellal *et al.* 2015). Established or emerging methods for Hg remediation do already exist using physical, chemical or biological routes (Guney *et al.* 2020). Among them, nano-FeS and $\gamma$-$Fe_2O_3$ (Ramezani *et al.* 2016) can be used to immobilize Hg but an additional step is necessary to convert $Hg^{2+}$ into $Hg^0$.

Both ZVI and magnetite have the potential to reduce aqueous $Hg^{2+}$ according to three basic redox reactions (standard redox potentials are from White & Peterson (1996) and Bard *et al.* (1985)):

$$Hg^{2+}, aq + Fe^0 \Rightarrow Hg^0 + Fe^{2+}, aq \rightarrow \Delta E^0 = 1.30\ V \quad (1)$$

$$Hg^{2+}, aq + 2[Fe^{2+}]_{Fe_3O_4} \Rightarrow Hg^0 + 2[Fe^{3+}]_{Fe_2O_3} \rightarrow 0.2\ V < \Delta E^0 < 0.5\ V \quad (2)$$

$$Hg^{2+}, aq + 2Fe^{2+}, aq \Rightarrow Hg^0 + 2Fe^{3+}, aq \rightarrow \Delta E^0 = 0.09\ V \quad (3)$$

White & Peterson (1996) showed that the half-cell potential for solid-state oxidation of ferrous iron in magnetite, noted $[Fe^{2+}]_{Fe3O4}$ in R.2, into ferric iron in maghemite, noted $[Fe^{3+}]_{Fe2O3}$ in R.2, falls in the −0.35 to −0.65 V range. This means that magnetite (R.2) is a stronger reducing agent than aqueous $Fe^{2+}$ (R.3). Homogeneous reduction of $Hg^{2+}$ by aqueous $Fe^{2+}$ according to R.3 has been reported experimentally (Amirbahman *et al.* 2013) and was shown to be catalyzed by the presence of hematite and goethite surfaces.

The reduction kinetics of aqueous $Hg^{2+}$ into $Hg^0$ according to R.2 has been studied by Wiatrowski *et al.* (2009) and was found to follow a pseudo first-order rate law. The kinetics is favored by increasing pH in the 4.8–6.7 range, increasing magnetite surface area and decreasing chloride concentration. For an $Fe_3O_4$ surface area of 2 $m^2\ L^{-1}$, over 80% of the measured $Hg^{2+}$ loss (100 nM $HgCl_2$) occurred in less than 15 min. Electron transfer between iron and mercury is believed to proceed through an $Hg^{2+}$ adsorption step onto the magnetite surface.

The removal rate of aqueous $Hg^{2+}$ by nanoparticles of zerovalent iron (nZVI) supported on pumice, i.e. according to R.1, has been investigated by Liu *et al.* (2014) in the 3.11–8.13 pH range. With a nZVI surface area of 32.2 $m^2\ g^{-1}$ (BET), above 98% of $Hg^{2+}_{aq}$ (60 mg $L^{-1}$) removal was achieved within minutes. High-resolution XPS showed a short $Hg^{2+}$ adsorption step (<30 sec) onto nZVI surface before it was reduced into $Hg^0$. Using nZVI (30 $m^2\ g^{-1}$, 2 g $L^{-1}$), Yan *et al.* (2010) obtained 98% of aqueous $Hg^{2+}$ (40 mg $L^{-1}$) removal in 2 min. At the nanoscale, Yan *et al.* (2010) showed using X-ray energy-dispersive spectroscopy (XEDS) that nZVI particles are composed of a metallic-iron core surrounded by a thin disordered oxide layer (core-shell model). Only $Hg^0$ could be observed with XPS at the nZVI surface confirming the possibility of Hg remediation by adsorption–reduction. The authors obtained much lower removal efficiencies with a larger particle size of 4.1 μm.

As shown in the studies cited above, the removal of $Hg^{2+}$ in aqueous media by metallic iron and/or magnetite proceeds with characteristic reaction times in the order of minutes. The characterization of the dynamics of aqueous $Hg^{2+}$ reduction requires appropriate analytical tools with suitable time response. Monitoring these dynamics through time-resolved solution sampling or time-resolved $Hg^0$ gold-trapping is not convenient since it requires frequent (~0.1–1 $min^{-1}$) and numerous

sampling and, therefore, a multiplication of analyses. Here, we used an automated mercury vapor analyzer based on atomic absorption with a sampling frequency of 0.2 $min^{-1}$ to investigate the dynamics of $Hg^0$ production induced by the interaction between aqueous $Hg^{2+}$ and the composite M/ZVI powder.

## METHODOLOGY

### Magnetite starting material

Magnetite starting material was synthesized from the corrosion of reagent grade iron beads (ZVI, Alfa Aesar – 00737, ≥99%, 2.8 μm diameter) at 200 °C in a 1 M solution of acetic acid in a stainless-steel autoclave. Temperature was measured to within ±1 °C with a K-type thermocouple plunging in the solution. The reactor was stirred at 200 rpm. Pressure was used to monitor the reaction progress and was measure with a pressure transducer. A total pressure increase of >10 MPa was measured which combined the effect of both heating and $H_2$ production associated with $3\ Fe^0 + 4\ H_2O = Fe_3O_4 + 4\ H_2$ reaction. At the end of the experiment, the reactor was cooled at around 0.6 °C $min^{-1}$. The run product was rinsed with ultrapure water, separated magnetically from the run solution, and dried at 50 °C for 24 h. Part of the product was placed on a double-sided carbon tape and carbon coated for imaging with scanning electron microscopy (SEM), another part was ground under ethanol for X-ray powder diffraction. SEM image analysis performed on 150 particles from the run products yielded a mean particle size (and standard deviation) of 2.6 ± 1.6 μm (Figure 1). Quantitative X-ray diffraction using the BGMN software (Doebelin & Kleeberg 2015) showed that the corrosion product was composed of magnetite with around 8 wt.% of residual Fe metal (Fig. S1). The BET surface area of the starting ZVI beads and of the experimental product was measured with $N_2$ gas and was found to be 0.4 and 9.0 $m^2\ g^{-1}$, respectively.

### Titration experiments

M/ZVI dissolution rate at constant pH (4 or 6) was measured by pH metric titration under $N_2$ bubbling using an automated titrator (716 Titrino, Metrohm) operated by Tiamo™ 2.3 software (Metrohm). One hundred and fifty milliliters of degassed NaCl solution at $10^{-3}$ M was adjusted at a fixed pH (4 or 6) with HCl. Then, 1.5 g of M/ZVI was added and the pH was maintained constant by automated addition of HCl (0.1 or 0.01 M, respectively). Both pH and volume of added acid were recorded.

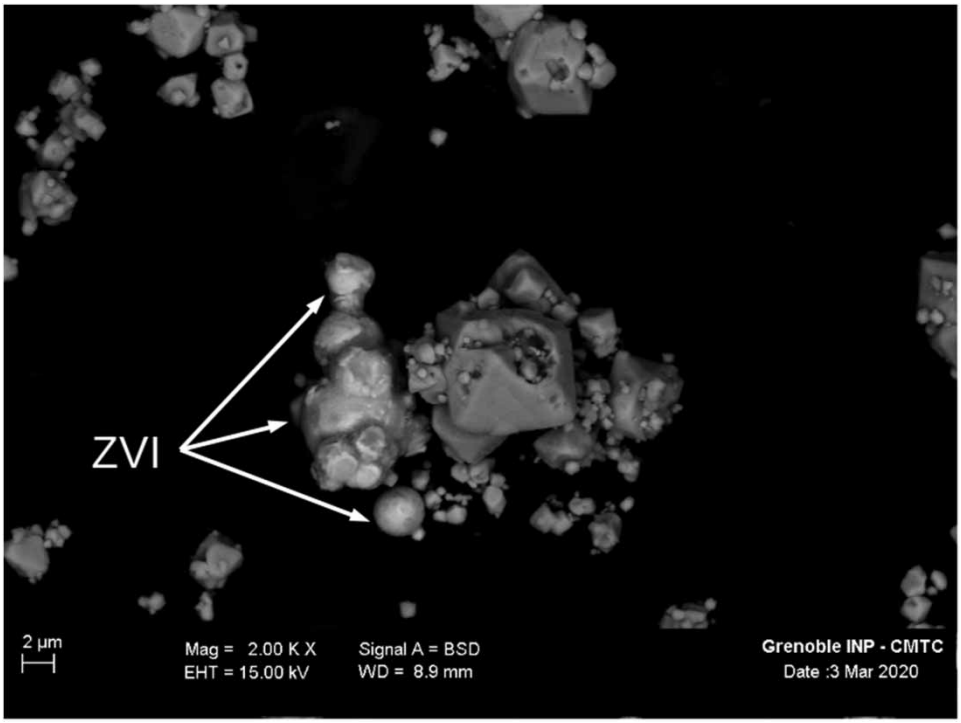


**Figure 1** | Back-scattered electron image of the M/ZVI product. Euhedral magnetite grains have sizes comprised between a few hundreds of nm to almost 10 μm. Residual ZVI beads are indicated by arrows on the SEM image.

Aqueous iron concentration was determined on 2 mL solution samples. Magnetite particles were separated from the sampled solution with a magnet and the solution was centrifuged (5 min at 13,000 rpm) and filtered to 0.025 μm. The aqueous $Fe^{2+}$ and $Fe_{tot}$ concentrations were derived using the o-phenanthroline spectrophotometric method (Herrera *et al.* 1989) at 511 nm with a spectrophotometer Lambda 35 Perkin Elmer. [$Fe^{3+}$] was deduced from [$Fe_{tot}$]-[$Fe^{2+}$].

### Experimental set-up and $Hg^0$ analyzer

The experimental set-up (Fig. S2) was composed of a 500 mL brown glass reactor in series with a 60 mL brown glass flask. The gas flux was monitored by a 0–325 mL $min^{-1}$ argon (Ar) glass-tube flow-meter placed upstream. The Ar tightness of the set-up was checked using a second flow-meter as outlet. All connections were made with fluoroethylen propylene (FEP) tubing to minimize gas adsorption and with silicone tubing at some points to ensure air tightness. The stirred glass reactor was closed tight with a screw cap equipped with a silicon/FEP septum. Three 3 mm diameter holes were pierced in the septum to insert FEP tubes, themselves inserted into silicon tubes over the width of the septum. A first outlet was connected to a polycarbonate Luer shut-off valve to allow solution sampling. A second outlet was used for $Hg^0$ outflow under Ar stream and was connected to the 60 mL condensation flask placed in an ice bath. The plug and the FEP and silicon tubes of the condensation flask through the silicon/FEP septum were designed similarly to those of the reactor but with two holes inside the septum for both $Hg^0$ inflow and outflow. The outlet gas flow was filtered through a 60 mm Whatman® Vacu-Guard® 0.45 μm polytetrafluoroethylene (PTFE) inline membrane (Fig. S2) before it was analyzed by the Gardis device. The mercury analyzer cycle started with pumping the Ar gas for 90 s. Elemental Hg accumulated on two 99.99% pure gold traps following a 'dual amalgamation' process which was selective to $Hg^0$. A thermo-desorption stage then followed which lasted for 60 s at 10 mL $min^{-1}$ using a Ni-Cr wire wrapped around the gold trap for heating. The desorbed $Hg^0$ passed through a two-optical beam for absorption measurements at 254 nm. At the end of the measurement cycle, a cooling step of 2 min was applied during which the analyzer was bypassed and the gas was then directed to the external gold trap. Operating conditions were optimized to obtain (i) the maximum $Hg^0$ flow inside the analyzer and avoid the reactor to be under pressure and (ii) the highest $Hg^0$ sensitivity when the lowest volume (0.2 μL) of $Hg^0$ saturated vapor was injected for calibration. With an input Ar flow rate of 75 mL $min^{-1}$, the gas sampling flow rate was tuned to around 52 mL $min^{-1}$ for a sampling time of 90 seconds. It should be noted that with an inflow rate of 75 mL $min^{-1}$, the gas contained in the head-space of the reactor was renewed every 2–3 minutes.

The sample powder was reacted with 300 mL of a $Hg^{2+}$ solution under stirring with a magnetic bar. The reactor was equipped with a glass bubbler to ensure fine Ar inflow into the solution. The outlet gas flow was analyzed every 5 min using a cold vapor atomic absorption spectrometry (CV-AAS) automated Mercury analyzer (Gardis-5®). This type of analyzer is able to detect down to 0.5 pg $Hg^0$ vapor (Urba *et al.* 1995). The gas which did not flow through the Gardis-5® analyzer was collected in a sandy gold trap for further analysis using CV-AFS (see next section).

$Hg^0$ background signal was collected in a set of blank experiments as well as at the beginning of all experiments prior to the powder sample injection. The Gardis baseline (~1–3 pg) was first determined using pure water and by monitoring $Hg^0$ in the set-up using the same experimental conditions as for all other experiments (90 second sampling, Ar inflow rate 75 mL $min^{-1}$).

### Complementary Hg analyses

Elemental Hg that was not sampled (and analyzed) with the Gardis-5® device, i.e. mainly during the Gardis-5® cooling stage of 2 min, was trapped on an external sandy gold-trap (Fig. S2). The $Hg^0$ trapped on the external gold-trap was desorbed on the day the experiment ended in a pre-cleaned (500 °C, 1 h) opaque flask containing 10 mL of 5 mM $KMnO_4$ (Hg < 0.000005%) in 5% pure $HNO_3$ (Optima™, Hg < 50 pg $g^{-1}$). Desorption was achieved by repeated heating (10 times) of the external gold trap according to cycles of 13 seconds using an induction coil under a flow of 99.999% Ar gas. Hg content of the $KMnO_4$ solution was further quantified using a CV-AFS with a protocol based on BrCl oxidation, $SnCl_2$ reduction, $Hg^0$ amalgamation and detection by atomic fluorescence at 254 nm with a detection limit of 0.1 ng $L^{-1}$.

Additional Hg remaining in the system, either in the solution, adsorbed onto the residual powder or onto the reactor walls as well as aqueous $Fe^{2+}$, were quantified in selected experiments. Samples for Hg analysis were stored in acid-cleaned FEP Teflon bottles following ultra-clean techniques (Bloom 1995), acidified with Rotipuran® HCl (Hg < 50 ng $L^{-1}$) and kept at 4 °C until analysis.

Recovered solutions were acidified at 0.5% (v/v) (Parker & Bloom 2005). A 1 mL aliquot was complexed with 2 mL of a pH 4.5 buffer and 2 mL of $6.0 \times 10^{-3}$ M o-phenantroline for $Fe^{2+}$ quantification. Hg adsorbed on the sample powder and on the

gas frit was recovered by leaching both magnetic stirrer bar and gas frit in 50% (v/v) HCl under ultrasonic bath for 30 min. The Hg contribution of acid and glassware was determined using the same conditions of leaching in ultra-pure water. Reactor walls were reacted with 300 mL of 10% (v/v) HCl for at least 24 h, and the recovered solution was analyzed for Hg after filtration through polyvinylidene difluoride 0.45 μm membranes.

The pH of the reacting Hg solution was determined with a Metrohm 781 pH-meter at the beginning (*Start pH*, Table 1) and at the end of the experiments (*End pH*, Table 1). In Run 2-7, pH was measured with the pH meter of the automated titrator. For the *Start pH* measurement, the solution was sampled several minutes after the beginning of the experiment, i.e. when the Ar inflow had begun and the sample powder had not yet been introduced. The experiment was considered to start at $t_0$ when the sample was introduced.

## RESULTS

### M/ZVI dissolution kinetics at pH 4 and 6 from HCl titration

Titration of M/ZVI was performed at pH 4 which has been the starting pH for most monitoring experiments of $Hg^0$ production. The volumetric HCl addition followed three main steps (1, 2 and 3 on Figure 2). First, around $4 \times 10^{-3}$ mole HCl was introduced within 1 hour ($4 \times 10^{-3}$ mole $h^{-1}$). Then, automated HCl addition rate decreased down to $2.3 \times 10^{-3}$ mole $h^{-1}$. After 5.5 hours of titration, automated HCl addition mostly stopped (Step 3). Overall, a total of $1.2 \times 10^{-2}$ moles of HCl was added.

A similar succession of steps could be inferred from the evolution of $[Fe^{2+}]$ in the solution (Figure 2). After 19 hours, a total of $5.8 \times 10^{-3}$ mole of iron had been released into the solution corresponding to a ca. 2:1 molar ratio between added HCl and $Fe^{2+}$, aq as expected from electroneutrality under constant pH:

$$2[Fe^{2+}] + [H^+] = [Cl^-] + [OH^-] \quad (4)$$

The amount of aqueous $Fe^{3+}$ was around two orders of magnitude less concentrated than $Fe^{2+}$. X-ray diffraction of the residual powder after titration indicated that all ZVI was consumed. The amount of aqueous $Fe^{2+}$ after Step 1 of $4 \times 10^{-3}$ mole (Figure 2) roughly corresponds to the number of moles of $Fe^0$ in the solid sample. Therefore, Step 1 can be attributed

**Table 1** | List of experiments with online monitoring of the $Hg^0$ production

| Run | Reactor type | Start pH | End pH | Duration (h) | m start. mat. (mg) | $[Fe^{2+}]$ (mg $L^{-1}$) | $H_2O$ vol. (ml) | $[Hg^{2+}]$ start (ng/l) | $[Hg^{2+}]$ end (ng/l) | Tot. $Hg^0$ (pg) |
|---|---|---|---|---|---|---|---|---|---|---|
| *M/ZVI* | | | | | | | | | | |
| 2_1* | 1 | 4.16 | 4.8 | 20.4 | 10.3 | 3.8 | 285.3 | 28.8 | 7.4 | 3553 |
| 2_2 | 1 | 4.2 | 6.1 | 68.7 | 10.3 | 2.5 | 289.1 | 27.8 | 3.4 | 4142 |
| 2_3 | 1 | 2.1 | 2.2 | 22.0 | 10.3 | 3.6 | 287.1 | 25.4 | 2.3 | 704 |
| 2_4 | 1 | 3.7 | 7.9 | 21.4 | 10.1 | 0.2 | 289.6 | 24.6 | 2.2 | 11547 |
| 2_5 | 1 | 5.1 | 7.4 | 47.9 | 10.7 | 0.2 | 291.2 | 24.1 | 1.3 | 2872 |
| 2_6** | 1 | 4.2 | 7.0 | 21.4 | 10.6 | 1.5 | 284.3 | 23.8 | 0.6 | 3336 |
| 2_7 | 2 | 4.2 | 6.8 | 23.9 | 10.5 | 2.1 | 300.8 | 23.6 | 0.8 | 3326 |
| 2_8 | 2 | 4.1 | 4.2 | 23.0 | 0.0 | n.d. | 302.1 | n.d. | n.d. | n.d. |
| 2_12 | 1 | 4.4 | 5.7 | 68.2 | 12.3 | 5.2 | 280.2 | 40.5 | 0.3 | 4589 |
| *ZVI* | | | | | | | | | | |
| 2_9 | 2 | 4.2 | 6.8 | 19.4 | 1.4 | 3.0 | 298.6 | 23.8 | 3.2 | 2658 |
| 2_11 | 1 | 3.9 | 8.0 | 41.9 | 21.6 | 2.9 | 290.7 | n.d. | n.d. | n.d. |
| 2_11bis | 1 | 6.6 | 7.5 | 28.0 | 10.4 | 0.7 | 274.5 | n.d. | n.d. | n.d. |
| 2_13 | 1 | 4.6 | 6.4 | 16.7 | 10.4 | 0.5 | 285.5 | n.d. | n.d. | n.d. |

Reactor type: (1) Opaque glass flask (592 mL); (2) Transparent glass wrapped in Al foil (547 mL).
Footnote: *with NaN3 ($10^{-3}$ M); **Hg supplied as $Hg(NO_3)_2$.

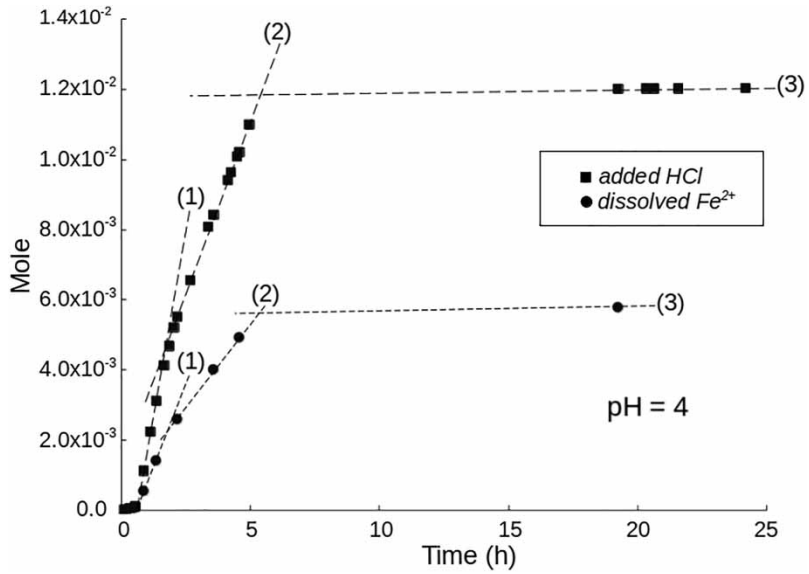


**Figure 2** | pH-metric titration of the M/ZVI product and iron release rate. pH was set to 4 and the titration was performed using 0.1 M HCl. Upper curve corresponds to added HCl moles and black dots are [$Fe^{2+}$] data. Three successive dissolution steps can be distinguished, labeled (1), (2) and (3).

to the anoxic dissolution of ZVI at rate of $2 \times 10^{-3}$ mole $h^{-1}$ (pH = 4):

$$Fe^0 + 2H^+ \rightarrow Fe^{2+}, Aq + H_2 \quad (5)$$

Automated titration of the M/ZVI product has also been performed at pH 6 over 26 hours (Suppl. Fig. S3). Dissolution was by two to three orders of magnitude slower than at pH 4 and occurred in a discontinuous manner (Fig. S3). In a first step (Zone 1, Fig. S3), HCl was added at a maximum rate of ca. $1.5 \times 10^{-5}$ mole $h^{-1}$ within the first 2 hours. This first step was followed by a second step with almost no HCl addition (Zone 2) which finally resumed after 3 hours (Zone 3) at a rate of $0.5 \times 10^{-6}$ mole $h^{-1}$ until the titration was terminated at $t_0 + 25$ h. At $t_0 + 19$ h, the solution was sampled and contained only $7.0 \times 10^{-6}$ mole of $Fe^{2+}$ corresponding to the anoxic dissolution of only 260 mg per kg of ZVI. X-ray powder diffraction of the residual M/ZVI powder after the experiment confirmed that most of the initial ZVI was still present. The $Cl^-/Fe^{2+}$ molar ratio in the solution was close to 1.6 and therefore departed from the expected ratio of 2 as predicted by Equation (4). This discrepancy is not accounted for by the presence of aqueous ferric iron which was not present in significant amounts since [$Fe^{2+}$]~[$Fe_{tot}$].

### Patterns of $Hg^0$-Gardis production events and effect of pH

A total of five blank experiments was carried out which are detailed in the supplementary data (Fig. S4). These blanks showed that neither ZVI nor M/ZVI was an intrinsic source of $Hg^{2+}$. Therefore, any $Hg^0$ production event that would occur after sample introduction corresponded to mercury that came from the solution. They also demonstrated that $NaN_3$ cannot be at the origin of measured $Hg^0$ production events. Furthermore, aqueous $Fe^{2+}$ was not found to produce $Hg^0$ in the 2.3–9 pH range. Small $Hg^0$ production events (<10–15 pg) were associated with NaOH addition which occurred to contain minor Hg.

Besides these blank experiments, time-resolved $Hg^0$ production was monitored during the reaction of M/ZVI with $Hg^{2+}$ solutions, prepared from $HgCl_2$ or $Hg(NO_3)_2$, with concentrations between 20 and 40 ng $L^{-1}$ (Table 1). Various patterns of $Hg^0$ production events were recorded which appeared to be strongly dependent on the pH evolution in the course of each experiment.

Experiment 2-1 (*Start pH* = 4.2) was the only experiment that was performed with $NaN_3$ (pKa = 4.6, 10 mM) which is a bacterial activity inhibitor (Ingledew & Poole 1984; Hochstein & Tomlinson 1988; Hendrix *et al.* 2019). The idea was to test whether the $Hg^0$ production events could relate to bacterial activity. In the course of Run 2-1, pH only varied within the 4–5 range due to the buffering effect of $NaN_3$. The $Hg^0$ Gardis production pattern of Run 2-1 (Figure 3(a)) was

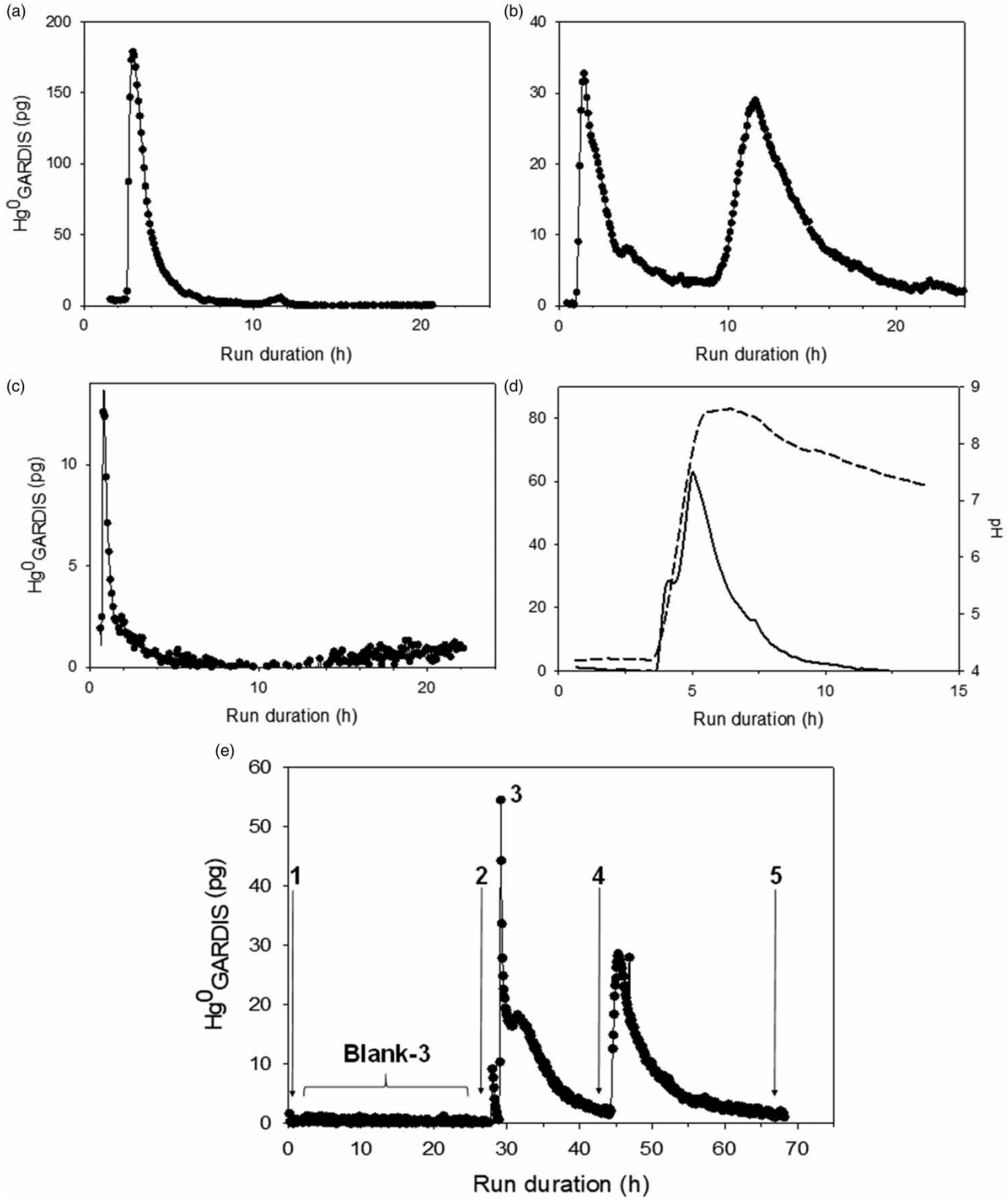


**Figure 3** | Typical $Hg^0$ - Gardis production pattern. (a) Run 2-1 in a $10^{-3}$ M $NaN_3$ solution, (b) Run 2-2 where pH drifted to a value above 6 in the course of the experiment, (c) Run 2-3 at pH of *ca*. 2 after addition of $1.5 \times 10^{-3}$ mole $HNO_3$. (d) Run 2-7 with time-resolved $Hg^0$ Gardis (plain curve) and pH monitoring (dashed curve). (e) Run 2-12 with selective ZVI dissolution to investigate single-phase magnetite behavior. At Point 1, pH was adjusted to 4.3 and 12.3 mg of M/ZVI was added. pH was maintained at 4.3 by HCl addition until ZVI dissolution. Once pH did no longer increase, Hg was added to 25 ng $L^{-1}$ (Point 2) which produced a small $Hg^0$ peak that was always encountered after $Hg^{2+}$ addition. The $Hg^0$ Gardis production peak at Point 3 occurred after the pH was increased from 4.3 to 6.3. pH decreased down to 5.7 as measured at Point 4 at which 25 ng $L^{-1}$ of Hg was added again. At Point 5, pH was still 5.7.

characterized by a strong $Hg^0$ production event which occurred 37 min after the M/ZVI sample was dropped into the reactor. This event led to the reduction of around half of the initial $Hg^{2+}_{aq}$ and was not related to bacterial activity.

Another typical $Hg^0$ production pattern was encountered in M/ZVI experiments to which no $NaN_3$ was added and for which pH drifted to values above 6 in the course of the measurements. For example, Run 2-2 showed a sharp $Hg^0$ production peak (Figure 3(b)) about 22 min after the introduction of M/ZVI, followed after around 8.5 hours by a second main $Hg^0$ production peak which spread over around 10 h. This typical pattern with a first $Hg^0$ production peak followed by a wide (and sometimes multiple) peak was basically encountered in every experiment where the *End pH* was above 6. It should be noted that the second reduction event did not always occur at the same time in the course of an experiment.

In order to relate $Hg^0$ production to pH evolution, both parameters were simultaneously monitored in Run 2-7 (Figure 3(d)). A first $Hg^0$ production event was observed in the form of a shoulder on the main $Hg^0$ production peak, immediately after M/ZVI was dropped in the reaction flask. Within less than an hour, pH increased to its maximum value (pH ~ 8.5). The maximum $Hg^0$ production rate coincided with the pH maximum. The slow pH decrease observed after aqueous $Hg^{2+}$ had been reduced can be related to the slow oxidation of aqueous $Fe^{2+}$ due to the flow of Ar gas which contained around 5 ppmv of $O_2$. Indeed, in 10 h, an $O_2$ contamination of *ca.* $10^{-5}$ mole per liter of solution can be calculated which is of the same order of magnitude as the [$Fe^{2+}$] in the recovered solution (Table 1). In the early stage of the experiments, however, while ZVI was still present in the solid starting material, reducing conditions might have prevailed as imposed by the dissolution of ZVI (named $Fe^0$ in R.6) which can potentially consume $O_2$:

$$H_2O + Fe^0 + {}^1/_2\, O_2 \rightarrow Fe^{2+} + 2\, OH^- \tag{6}$$

### Effect of single-phase ZVI on Hg reduction dynamics

In order to decipher the specific role of ZVI in the composite M/ZVI powder with respect to $Hg^{2+}$ reduction, $Hg^0$ monitoring experiments were carried out independently with single-phased ZVI (Run 2-9, 2-11, 2-11bis). We used as starting material the ZVI compound (Alfa Aesar – 00737, ≥99%) from which M/ZVI was synthesized. In all reduction experiments with ZVI, $Hg^0$ production was significant and observed shortly after ZVI introduction, in the form of a sharp $Hg^0$ Gardis peak. After each $Hg^0$ production event, [$Fe^{2+}$] and pH (from 5.2 to 7.9 in Run 2-11; from 5.9 to 7.8 in Run 2-11bis) both increased.

Run 2-11 and 2-11bis were both performed by changing some of the experimental parameters in the course of the experiment itself taking advantage of the real-time monitoring of the $Hg^0$ production allowed by the Gardis analyzer. In 2-11, *Start pH* was adjusted to 3.9 and 10.6 mg of ZVI were introduced at $t_0$ in the 25 ng $L^{-1}$ $Hg^{2+}$ solution. After the first event of $Hg^0$ production, a pH of around 5.2 was measured ($t_0 + 18.4$ h) and [$Fe^{2+}$,aq] reached 0.31 mg $L^{-1}$ ($t_0 + 18$ h) meaning that around 1 wt.% of the ZVI had been dissolved. Further addition of 11 mg of ZVI ($t_0 + 19.1$ h) did not lead to further $Hg^0$ production confirming that the amount of available ZVI was not the limiting factor to $Hg^0$ production. The addition of 25 ng $L^{-1}$ of $Hg^{2+}$ to the solution ($t_0 + 22.7$ h) triggered a sharp and intense $Hg^0$ Gardis peak (*ca.* 400 pg) at pH around 5.2.

We show here that in the conditions of the 2-11 experiment with 10 mg of ZVI, the extension of the $Hg^0$ production event is limited by the amount of $Hg^{2+}$ and not by the amount of ZVI since ZVI addition does not lead to another $Hg^0$ production event. The corresponding reduction process was effective and fast at pH 4 and 5.2 (2 and 2.5 h, respectively). The anoxic dissolution of ZVI can drive the pH to values up to 8 as measured at $t_0 + 42$ h, *i.e*, at the end of the 2-11 experiment.

The 2-11bis experiment was basically similar to the 2.11 one but higher pH was investigated. The starting pH was adjusted to 6.6 and 10.5 mg of ZVI was added at $t_0$. $Hg^0$ was produced immediately as recorded on the Gardis device in the form of the sum of two overlapping peaks. At $t_0 + 23$ h, pH reached 8.5 and another 25 ng $L^{-1}$ of $Hg^{2+}$ was added to the solution which immediately resulted in a major $Hg^0$ Gardis production peak (*ca.* 500 pg amplitude). pH was then decreased down to 5.4 and another 25 ng $L^{-1}$ of $Hg^{2+}$ was added ($t_0 + 28$ h) and, again, a major $Hg^0$ Gardis event was recorded with *ca.* 400 pg of amplitude.

### Effect of single-phase magnetite on Hg reduction dynamics

The specific role of magnetite in the $Hg^{2+}$ reduction process was tested on the M/ZVI product after complete removal of its ZVI component by selective dissolution. The dissolution of ZVI, which is far more soluble than magnetite, was achieved in the experimental setup itself in order to avoid unnecessary handling and associated contamination/oxidation. In the 2-12 experiment (Figure 3(e)), 12.3 mg of the M/ZVI product was introduced in the reactor containing a Hg-free solution at pH 4.3. The pH rise which was associated to the selective dissolution of the ZVI component, was compensated by successive

additions of $HNO_3$ until pH no longer increased and remained equal to 4.3. This constant pH regime was interpreted as the complete dissolution of the ZVI component. At this stage, $[Fe^{2+}]$ reached 6.5 mg $L^{-1}$. This concentration is actually higher than expected in the case of the dissolution of all ZVI (8 wt.%) contained in the starting M/ZVI, partial dissolution of the magnetite component must thus also be considered. At $t_0 + 28$ h, $Hg^{2+}$ was added to reach a concentration of 25 ng $L^{-1}$ in the reactor. A small and sharp $Hg^0$ production event was then recorded (amplitude *ca.* 10 pg). This type of small amplitude event was systematically recorded when $Hg^{2+}$ was added to the experimental solution and likely reflects an increase of the $Hg^0$ partial pressure according to Henry's law. Then, pH was increased to 6.3 which triggered a large $Hg^0$ production event that lasted around 10 hours. Once the $Hg^0$ Gardis signal returned below 2 pg, pH was 5.6 and another 25 ng $L^{-1}$ of $Hg^{2+}$ was added. This, again, triggered $Hg^0$ production, indicating that the previous $Hg^0$ production steps consumed all the $Hg^{2+}$ that was available for reduction.

### Magnitude of the Hg reduction

The proportion of initial Hg that is reduced and trapped on both Gardis and the external gold trap was determined for a selection of experiments (Table 2) and was found to amount to around 40–50%. The amount of $Hg^{2+}$ that remained in the solution at the end of the experiment was typically between 5 and 15%. Since particles can be sampled with the solution which was not filtrated, this proportion should be seen as an upper bound of the final $[Hg^{2+}]$. Indeed, it can be noted that the solution of Run 2-12 which has been filtrated displays the lower Hg content ($[Hg^{2+}]_{end}$, Table 1). The Hg adsorbed onto both residual solid sample and gas frit was found to represent another 30% of the initial Hg (Table 2). Finally, part of the Hg was adsorbed onto the flask walls to a level of ca. 15% as determined on the 2-12 experiment.

## DISCUSSION

### Limitations of the set-up for monitoring aqueous $Hg^{2+}$reduction

The experimental set-up that was designed in this study allowed the identification of $Hg^0$ production events that typically proceeded at the hour timescale. The frequency of the $Hg^0$ analysis with the Gardis-5® (0.2 $min^{-1}$) allowed a good resolution of these $Hg^0$ production events. It can thus be concluded that the set-up is well-suited to investigate the $Hg^0$ production dynamics by magnetite- and ZVI-based materials. At this stage, however, the $Hg^0$ Gardis measurement does not provide an accurate evaluation of the total $Hg^0$ that is produced in the experiments. The proportion of total $Hg^0$ that was trapped and analyzed by the Gardis device could basically vary by a factor of two from one experiment to another although it should be reproducible for identical sampling procedure and gas flow rate. Possible variations in Ar gas flow might be invoked, either Ar inflow variations in the whole system or in the gas analyzer upon automatic pumping. Therefore, only the order of magnitude of the total $Hg^0$ produced could be inferred at this stage and $Hg^0$ Gardis data can only be considered as a semi-quantitative estimate of the total amount of $Hg^0$ that was actually produced.

Being aware of that limitation, we show here that the composite powder obtained from the corrosion of iron metal powder and consisting in a mixture of magnetite (M) and residual iron metal (ZVI) was effective to reduce aqueous $Hg^{2+}$ in the 4–8.5 pH range. The sensitivity of the Gardis analyzer made it possible to probe $Hg^0$ production at the picogram level. In order to avoid memory effects on the Gardis analyzer encountered when $Hg^0$ exceeds amounts in the order of 160 pg, the mass of starting M/ZVI was minimized down to a level (ca. 10 mg) at which it could still be accurately weighed and an initial $[Hg^{2+}]$ of 25 ng $L^{-1}$ was chosen. The quantity of Hg adsorption sites on the surface of magnetite in the present experiments was close to 6 nmole of sites per liter considering an adsorption site density at the surface of $Fe_3O_4$ of ca. $3.5 \times 10^{-5}$ mole $m^{-2}$ (e.g. Wesolowski *et al.* 2000; Missana *et al.* 2003). This concentration of adsorption sites is to be compared to the $[Hg^{2+}]$

**Table 2** | Hg distribution in selected experiments

| Run | $Hg^0$-GARDIS (pg) | $Hg^0$-Trap (pg) | Magnetite (pg) | Reactor wall (pg) | Recovery (%) |
|---|---|---|---|---|---|
| 2_2 | 2080 | 2062 | 1762 | n.d. | 85 |
| 2_9 | 668 | 1990 | 2174 | n.d. | 81 |
| 2_12 | 3709 | 880 | 2258 | 1975 | 78 |

The recovery (%) is defined as the total Hg after the experiment divided by the total Hg introduced in the system initially. Note that the solution of Run 2-12 has been filtrated and thus Hg associated with the filtrated particles is not accounted for by in the recovery.

which amounts to around 125 pmole $L^{-1}$ in our experimental solutions. For comparison, in their $Hg^{2+}_{aq}$ reduction experiments with magnetite, Wiatrowski *et al.* (2009) used a site concentration that was only two times higher and around 80 nmole $L^{-1}$ of aqueous $Hg^{2+}$ could be reduced. Therefore, the Hg reduction investigated here proceeded at only a few percent of the reduction capacity of magnetite present in M/ZVI. The [$Hg^{2+}$] was thus the limiting factor of $Hg^0$ production as confirmed by its reactivation after $Hg^{2+}$ addition in Run 2-12. Similarly, $Hg^0$ production in experiments performed with ZVI as starting material were also limited by the amount of aqueous $Hg^{2+}$ (Run 2-11 and 2-11bis).

Preliminary tests on solutions containing [$Cl^-$] comprised between 2 and 5 mmole·$L^{-1}$ (not shown here) with initial [$Hg^{2+}$] of 25, 75, 375 ng $L^{-1}$ and a M/ZVI mass of 10.1, 10.8 and 2.1 mg yielded a total $Hg^0$ production of 1020, 3320 and 4300 pg, respectively, showing a relatively good proportionality between produced $Hg^0$ and both initial quantities of M/ZVI and [$Hg^{2+}$].

## Dynamics of aqueous $Hg^{2+}$ reduction by M/ZVI

Titration experiments have shown that the dissolution of M/ZVI released aqueous iron which tended to increase the pH of the host solution. At pH 4 which was the starting pH of most $Hg^0$ monitoring experiments, ZVI was found to dissolve preferentially. At pH 6, the dissolution rate of M/ZVI was three orders of magnitude slower. When transposed to the $Hg^0$ monitoring experiments where pH was not buffered (apart for Run 2-1 containing $NaN_3$), it is thus expected that the pH increase due to M/ZVI dissolution will slow down with time until it reaches its final value.

[$Fe^{2+}$] at the termination of all experiments was found to vary between 2.5 and 4 mg $L^{-1}$ corresponding to a mass of dissolved iron of around 0.7–1.1 mg, i.e. between 7 and 11 wt.% of the starting material. Since ZVI represented around 8 wt.% of the starting material and since titration data at pH 4 showed that ZVI dissolved preferentially, it can be concluded that (1) the main contribution to the pH increase was the anaerobic dissolution of ZVI through the production of hydroxide ions ($Fe^{\circ}_{,solid} + 2\ H_2O = > Fe^{2+}_{,aq} + H_2 + 2\ OH^-$) and (2) all the ZVI in the starting material might have been consumed in our experiments.

The decrease in dissolution rate with increasing pH has been reported for both ZVI (Fu *et al.* 2014) and magnetite (Missana *et al.* 2003). In particular, Fu *et al.* (2014) indicated that iron release into the solution by ZVI particles becomes limited by the formation of a passivating hydroxide shell. Wilkin & McNeil (2003) have investigated the rate of removal of a series of heavy metals by ZVI at pH 2.3 and 4.5. They also observed an overall pH increase associated with ZVI dissolution. Actually, they could not define the removal rate for Hg since all the initial $Hg^{2+}$ had already been removed from the solution before their first [$Hg^{2+}_{aq}$] measurement. This type of fast kinetics is consistent with our observation for $Hg^{2+}$ reduction by ZVI.

Experiments with pure ZVI yielded a $Hg^0$ Gardis production pattern that was composed of a single event which could occur in a range of pH from 4 to 8.5 and possibly down to 2 according to Run 2-3 (Figure 3(c)).

By comparison, single phase magnetite did not reduce $Hg^{2+}_{aq}$ at pH 4.3 (Run 2-12) which was the starting pH of most experiments presented here. The production of $Hg^0$ by magnetite was triggered by the increase of pH up to 6.5 as attained in most experiments in response to ZVI dissolution mainly. We thus conjecture that $Hg^0$ Gardis patterns displaying two successive $Hg^0$ production events are the sum of the $Hg^{2+}$ reduction by ZVI followed by the reduction of remaining $Hg^{2+}$ at mild acidic pH.

The pH dependency of Hg reduction kinetics by stoichiometric magnetite has been established by Wiatrowski *et al.* (2009). The expected reduction rate for our experimental parameters were calculated with their data and are displayed in Figure 4 in the form of $Hg^0 = f(t)$ curves. It can be clearly seen (Figure 4) that at pH below 5, the $Hg^0$ production rate is associated with a broad peak of low intensity that will be barely resolved by the Gardis monitoring. At pH 6.5, a sharper $Hg^0$ Gardis peak should be produced with $Hg^{2+}$ reduction that proceeds within a few hours in good agreement with our observations.

Therefore, the respective role of the two components of the M/ZVI product with respect to $Hg^{2+}$ reduction can be summarized as follows. First, at pH 4, $Hg^{2+}$ is partly reduced to $Hg^0$ by ZVI which, in addition, shifts the pH of the solution to mild acidic values at which the $Hg^{2+}$ reduction rate by magnetite allows further reduction of $Hg^{2+}$ within a few hours.

The process of Hg reduction by ZVI in the form of nanoparticles is described as a core-shell model which involves $Hg^{2+}$ sorption onto an iron hydroxide shell which covers the nanoparticle and the reduction of $Hg^{2+}$ into $Hg^0$ by electron transfer from the ZVI core across the shell (Yan *et al.* 2010). This shell with a thickness from a few nanometers to 25 nm is commonly observed on ZVI nanoparticles (e.g. Yan *et al.* 2010; Crane *et al.* 2015). As expected for a surface-controlled process, Yan *et al.* (2010) showed that the Hg reduction rate decreases with ZVI particles having lower surface area. Martin *et al.* (2008) showed that the complete oxidation of nanoparticles of ZVI (50–100 nm) by aqueous $Cu^{2+}$ under near anoxic

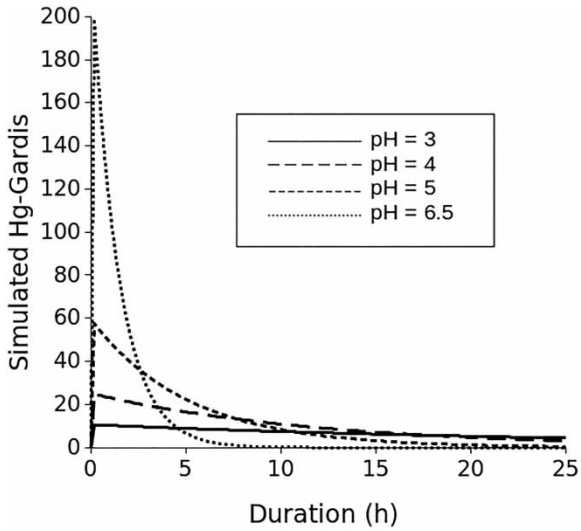


**Figure 4** | Simulation of $Hg^{2+}$ reduction kinetics by magnetite as a function of pH using the kinetics law by Wiatrowski *et al.* (2009). Total amount of [$Hg^{2+}_{aq}$] reduced and trapped on the Gardis is set to 6 ng $L^{-1}$ for the simulation.

conditions produces an iron oxide-hydroxide shell of around 3 nm. The reactivity of the nanoparticle is bounded to the thickness of the shell that can become passivating with respect to the core-shell reduction process (e.g. Wang *et al.* 2010). However, in the experiments performed here where ZVI dissolves and where pH increases consecutively, passivation might not be efficient since iron is continuously released into the solution. The dissolution rate of iron decreases with pH, as observed here at pH 6 compared to pH 4. Passivation by an oxide/hydroxide layer may then become relevant towards circumneutral pH. Actually, the stepwise dissolution of ZVI contained in M/ZVI observed at pH 6 in titration experiments (Fig. S3) could reflect the competition between passivation and dissolution. Such discontinuous dissolution implies that from pH 6 and above, the rate of pH increase is variable. This explains also why the second $Hg^0$ event which is attributed to magnetite once pH exceeds 6 occurs at different times in our experiments.

Whereas anaerobic dissolution of ZVI imposes reducing conditions (Sun *et al.* 2006), progressive decrease of the iron dissolution rate due to increasing pH will favor, in the presence of oxygen, the precipitation of iron oxide and/or hydroxide possibly as a shell around ZVI. The slow pH decrease observed on Figure 3(d) (Run 2-7) is the likely result of iron oxide/hydroxide slow precipitation due to the presence of $O_2$ as traces in the Ar gas. Actually, the presence of magnetite once circumneutral conditions have been attained will ensure that fast and efficient $Hg^{2+}$ reduction will proceed. A fraction of this magnetite can actually be produced by anaerobic corrosion of the ZVI (e.g. Odziemkowski *et al.* 1998) according to the same process that led to the hydrothermal production of the M/ZVI starting material from ZVI.

The pseudo-first order rate law established by Wiatrowski *et al.* (2009) for Hg reduction in the presence of $Fe_3O_4$ and its pH dependency are found to apply even to Hg solutions that are around 1000 times less concentrated than those used by the authors to establish their rate law. We showed that even at a $Hg^{2+}$ concentration of 25 ng $L^{-1}$, which is about 100 times below the maximum contamination level in drinking water recommended by the US Environmental Protection Agency, 30 mg $L^{-1}$ of M/ZVI is able to remove around 50% of this Hg by reduction into $Hg^0$ in addition to the fraction that was adsorbed onto the reactor walls and onto the M/ZVI product itself. Although much less soluble and less sensitive to oxygen than ZVI, magnetite can oxidize what potentially lowers the reduction rate of contaminants (Gorski *et al.* 2010). The higher reactivity of ZVI may prevent or delay magnetite oxidation by imposing anoxic conditions.

## CONCLUSION

Both ZVI and magnetite surfaces have the chemical ability to reduce aqueous $Hg^{2+}$ into $Hg^0$. However, the use of these compounds for $Hg^{2+}$ remediation in aqueous environments faces some intrinsic limitations. ZVI can lose its $Hg^{2+}$ reduction efficiency upon dissolution or surface oxidation, two processes that are likely to occur rapidly owing to the high metastability of ZVI. Magnetite on the other hand is chemically more stable. However, magnetite powders with surface area in the 5–100 $m^2$ $g^{-1}$ range are costly to produce at the industrial scale. The use of composite M/ZVI powders in acidic to

mild acidic polluted waters and possibly aqueous industrial wastes, may offer an interesting alternative to the use of either of its constitutive components alone. This is especially the case in acidic conditions under which the ZVI component reduces efficiently part of the $Hg^{2+}$. At the same time, the ZVI dissolves, thus shifting the pH above 6. At pH >6, the kinetics of $Hg^{2+}$ reduction by magnetite becomes optimal and magnetite takes over the reduction of $Hg^{2+}$. Indeed, the rate of aqueous $Hg^{2+}$ reduction by magnetite is actually nine times faster at pH 6.5 than at pH 4 (Wiatrowski *et al.* 2009). Therefore, a pH shift from 4 to 6.5 may allow the use of nine times less magnetite to achieve the same $Hg^{2+}$ removal rate. At constant magnetite mass, a magnetite product with a 9-fold lower specific surface area can be used, e.g. grains with a diameter of 200 nm instead of 25 nm.

The low-temperature hydrothermal process that was applied here to commercial $Fe^0$ for the synthesis of M/ZVI could also be applied to ZVI-based wastes from the steel industry in order to minimize the cost of the starting raw material. The M over ZVI ratio can be easily tuned by varying the duration of the production process. The obtained products can be tested with the experimental set-up developed here which consists in the online $Hg^0$ analysis of the gas bubbling in a simple glass reactor containing solutions with sufficiently low [$Hg^{2+}$] to remain harmless for the operator. It must be noted that further $Hg^0$ removal can be envisaged using available technology for elemental mercury capture from flue gas, some of them being based on materials prepared from by-products of the steel industry as well (Ma *et al.* 2019). The next step should be the investigation of the M/ZVI potential for Hg remediation in polluted soils. Indeed, the $Hg^0$ production kinetics observed here are not directly applicable to soils where mercury is expected to be strongly retained in the solid fraction (Liao *et al.* 2009) in particular in the presence of organic matter (Yin *et al.* 1997a, 1997b; Miretzky *et al.* 2005).

## ACKNOWLEDGEMENTS

Stéphane Guédron is warmly thanked for sharing his knowledge on Hg behavior for the design of the experimental set-up. Nathaniel Findling is acknowledged for collecting and analyzing the X-ray powder diffraction data. Andrius Urba is thanked for his technical advice on the Gardis-5 device. All chemical and diffraction data were obtained using devices managed by the *Géochimie & Minéralogie* analytical platform of ISTerre (Grenoble, France). Electron images were collected using the FE-SEM facility at CMTC (Grenoble, France).

## DATA AVAILABILITY STATEMENT

All relevant data are included in the paper or its Supplementary Information.

## CONFLICT OF INTEREST

The authors declare there is no conflict.

## REFERENCES

Amirbahman, A., Kent, D. B., Curtis, G. P. & Marvin-DiPasquale, M. C. 2013 Kinetics of homogeneous and surface-catalyzed mercury(II) reduction by iron(II). *Environmental Science & Technology* **47** (13), 7204–7213.

Bard, A. J., Parsons, R. & Jordan, J. 1985 *Standard Potentials in Aqueous Solution*. M. Dekker Inc., New York.

Bloom, N. S. 1995 Mercury as a case study of ultra-clean sample handling and storage in aquatic trace metal research. *Environmental Laboratory* **3–4**, 20–25.

Brunet, F. 2019 Hydrothermal production of $H_2$ and magnetite from steel slags: a geo-inspired approach based on olivine serpentinization. *Frontiers in Earth Science* **7**, 17.

Clarkson, T. W. & Magos, L. 2006 The toxicology of mercury and its chemical compounds. *Critical Reviews in Toxicology* **36**, 609–662.

Crane, R. A., Dickinson, M. & Scott, T. B. 2015 Nanoscale zero-valent iron particles for the remediation of plutonium and uranium contaminated solutions. *Chemical Engineering Journal* **262**, 319–325.

Crouzet, C., Brunet, F., Recham, N., Findling, N., Lanson, M., Guyot, F., Ferrasse, J.-H. & Goffé, B. 2017 Hydrogen production by hydrothermal oxidation of FeO under acidic conditions. *International Journal of Hydrogen Energy* **42** (2), 795–806.

Doebelin, N. & Kleeberg, R. 2015 Profex: a graphical interface for the Rietveld refinement program BGMN. *Journal of Applied Crystallography* **48**, 1573–1580.

Fu, F., Dionysiou, D. D. & Liu, H. 2014 The use of zero-valent iron for groundwater remediation and wastewater treatment: a review. *Journal of Hazardous Materials* **267**, 194–205.

Geneti, S. T., Mekonnen, G. A., Murthy, H. C., Mohammed, E. T., Ravikumar, C. R., Gonfa, B. A. & Sabir, F. K. 2022 Biogenic synthesis of magnetite nanoparticles using leaf extract of Thymus schimperi and their application for monocomponent removal of chromium and mercury ions from aqueous solution. *Journal of Nanomaterials* **2022**, 1–15.

Gil-Díaz, M., Rodríguez-Alonso, J., Maffiotte, C. A., Baragano, D., Millan, R. & Lobo, M. C. 2021 Iron nanoparticles are efficient at removing mercury from polluted waters. *Journal of Cleaner Production* **315**, 128272.

Gilmour, C. C., Podar, M., Bullock, A. L., Graham, A. M., Brown, S. D., Somenahally, A. C., Johs, A., Hurt Jr, R. A.Jr, ., Bailey, K. L. & Elias, D. A. 2013 Mercury methylation by novel microorganisms from new environments. *Environmental Science & Technology* **47** (20), 11810–11820.

Gilmour, C. C., Bullock, A. L., McBurnet, A., Podar, M. & Elias, D. A. 2018 Robust mercury methylation across diverse methanogenic Archea. *MBio* **9** (2), e02403–17.

Gorski, C. A., Nurmi, J. T., Tratnyek, P. G., Hofstetter, T. B. & Scherer, M. M. 2010 Redox behavior of magnetite: implications for contaminant reduction. *Environmental Science & Technology* **44** (1), 55–60.

Guney, M., Akimzhanova, Z., Kumisbek, A., Beisova, K., Kismelyeva, S., Satayeva, A., Inglezakis, V. & Karaca, F. 2020 Mercury (Hg) contaminated sites in Kazakhstan: review of current cases and site remediation responses. *International Journal of Environmental Research and Public Health* **17**, 8936.

Gusain, R., Gupta, K., Joshi, P. & Khatri, O. P. 2019 Adsorptive removal and photocatalytic degradation of organic pollutants using metal oxides and their composites: a comprehensive review. *Advances in Colloid and Interface Science* **272**, 102009.

Hellal, J., Guedron, S., Huguet, L., Schafer, J., Laperche, V., Joulian, C., Lanceleur, L., Burnol, A., Ghestem, J., Garrido F, P. & Battaglia-Brunet, F. 2015 Mercury mobilization and speciation linked to bacterial iron oxide and sulfate reduction: a column study to mimic reactive transfer in an anoxic aquifer. *Journal of Contaminant Hydrology* **180**, 56–68.

Hendrix, K., Bleyen, N., Mennecart, T., Bruggeman, C. & Valcke, E. 2019 Sodium azide used as microbial inhibitor caused unwanted by-products in anaerobic geochemical studies. *Applied Geochemistry* **107**, 120–130.

Herrera, L., Ruiz, P., Aguillon, J. C. & Fehrmann, A. 1989 A new spectrophotometric method for the determination of ferrous iron in the presence of ferric iron. *Journal of Chemical Technology & Biotechnology* **44** (3), 171–181.

Hochstein, L. I. & Tomlinson, G. A. 1988 The enzymes associated with denitrification. *Annual Reviews in Microbiology* **42**, 231–261.

Ingledew, W. J. & Poole, R. K. 1984 The respiratory chains of Escherichia coli. *Microbiology Reviews* **48**, 222–271.

Liao, L., Selim, H. M. & DeLaune, R. D. 2009 Mercury adsorption–desorption and transport in soils. *Journal of Environmental Quality* **38** (4), 1608–1616.

Liu, Y. & Wang, J. 2019 Reduction of nitrate by zero valent iron (ZVI)-based materials: a review. *Science of The Total Environment* **671**, 388–403.

Liu, T., Wang, Z.-L., Yan, X. & Zhang, B. 2014 Removal of mercury (II) and chromium (VI) from wastewater using a new and effective composite: Pumice-supported nanoscale zero-valent iron. *Chemical Engineering Journal* **245**, 34–40.

Ma, L., Han, L., Chen, S., Hu, J., Chang, L., Bao, W. & Wang, J. 2019 Rapid synthesis of magnetic zeolite materials from fly ash and iron-containing wastes using supercritical water for elemental mercury removal from flue gas. *Fuel Processing Technology* **189**, 39–48.

Martin, J. E., Herzing, A. A., Yan, W., Li, X., Koel, B. E., Kiely, C. J. & Zhang, W. 2008 Determination of the oxide layer thickness in core-shell zerovalent iron nanoparticles. *Langmuir* **24**, 4329–4334.

Miretzky, P., Bisinoti, M. & Jardim, W. F. 2005 Sorption of mercury (II) in Amazon soils from column studies. *Chemosphere* **60** (11), 1583–1589.

Missana, T., García-Gutiérrez, M. & Fernńdez, V. 2003 Uranium (VI) sorption on colloidal magnetite under anoxic environment: experimental study and surface complexation modelling. *Geochimica et Cosmochimica Acta* **67** (14), 2543–2550.

Mueller, N. C., Braun, J., Bruns, J., Černík, M., Rissing, P., Rickerby, D. & Nowack, B. 2012 Application of nanoscale zero valent iron (NZVI) for groundwater remediation in Europe. *Environmental Science and Pollution Research* **19** (2), 550–558.

Odziemkowski, M. S., Schuhmacher, T. T., Gillham, R. W. & Reardon, E. J. 1998 Mechanism of oxide film formation on iron in simulating groundwater solutions: Raman spectroscopic studies. *Corrosion Science* **40** (2), 371–389.

Parker, J. L. & Bloom, N. S. 2005 Preservation and storage techniques for low-level aqueous mercury speciation. *Science of The Total Environment* **337** (1), 253–263.

Ponder, S. M., Darab, J. G. & Mallouk, T. E. 2000 Remediation of Cr(VI) and Pb(II) Aqueous solutions using supported, nanoscale zero-valent iron. *Environmental Science & Technology* **34** (12), 2564–2569.

Ramezani, Z., Pourmand, N., Behfar, A. & Momeni, A. 2016 Removal and recovery of mercury from chlor-alkali petrochemical wastes using $\gamma$-$Fe_2O_3$ nanoparticles. *Applied Petrochemical Research* **6**, 403–411.

Sun, Y.-P., Li, X., Cao, J., Zhang, W. & Wang, H. P. 2006 Characterization of zero-valent iron nanoparticles. *Advances in Colloid and Interface Science* **120** (1), 47–56.

UN Environment 2019 *Global Mercury Assessment 2018*. United Nation Environmental Programme, Chemicals and Health Branch, Programme Chemicals and Health Branch Geneva, Switzerland. ISBN 978-92-807-3744-8.

Urba, A., Kvietkus, K., Sakalys, J., Xiao, Z., Lindqvist, O., 1995 A new sensitive and portable mercury vapor analyzer Gardis-1A. In: *Mercury as a Global Pollutant. Proceedings of the Third International Conference held in Whistler, British Columbia, July 10–14, 1994* (Porcella, D. B., Huckabee, J. W. & Wheatley, B., eds). Springer Netherlands, Dordrecht, pp. 1305–1309.

Wang, Q., Lee, S. & Choi, H. 2010 Aging study on the structure of $Fe^0$-nanoparticles: Stabilization, characterization, and reactivity. *Journal of Physical Chemistry C* **114** (5), 2027–2033.

Wesolowski, D. J., Machesky, M. L., Palmer, D. A. & Anovitz, L. M. 2000 Magnetite surface charge studies to 290 °C from in situ pH titrations. *Chemical Geology* **167** (1–2), 193–229.

White, A. F. & Peterson, M. L. 1996 Reduction of aqueous transition metal species on the surfaces of Fe(II) -containing oxides. *Geochimica et Cosmochimica Acta* **60** (20), 3799–3814.

Wiatrowski, H. A., Das, S., Kukkadapu, R., Llton, E. S., Barky, T. & Yee, N. 2009 Reduction of Hg(II) to Hg(0) by magnetite. *Environmental Science & Technology* **43** (14), 5307–5313.

Wilkin, R. T. & McNeil, M. S. 2003 Laboratory evaluation of zero-valent iron to treat water impacted by acid mine drainage. *Chemosphere* **53** (7), 715–725.

Yan, W., Herzing, A. A., Kiely, C. J. & Zhang, W. 2010 Nanoscale zero-valent iron (nZVI): aspects of the core-shell structure and reactions with inorganic species in water. *Journal of Contaminant Hydrology* **118** (3), 96–104.

Yin, Y., Allen, H. E., Huang, C. P. & Sanders, P. F. 1997a Adsorption/resorption isotherms of Hg(II) by soil. *Soil Science* **162** (1), 35–45.

Yin, Y., Allen, H. E., Huang, C. P., Sparks, D. L. & Sanders, P. F. 1997b Kinetics of mercury(II) adsorption and desorption on soil. *Environmental Science & Technology* **31** (2), 496–503.

Zhang, W. 2003 Nanoscale iron particles for environmental remediation: an overview. *Journal of Nanoparticle Research* **5**, 323–332.

First received 16 November 2021; accepted in revised form 1 July 2022. Available online 13 July 2022